International Journal of Remote Sensing, 2013
Vol. 34, No. 21, 7464–7473, http://dx.doi.org/10.1080/2150704X.2013.820003

Polar grid fraction as an estimator of montane tropical forest canopy structure using airborne lidar

Nicholas R. Vaughn[a,b]*, Gregory P. Asner[b], and Christian P. Giardina[a]

[a]*Institute of Pacific Islands Forestry, USDA Forest Service, Hilo, HI 96720, USA;* [b]*Department of Global Ecology, Carnegie Institution for Science, Stanford, CA 94305, USA*

(*Received 26 February 2013; accepted 22 June 2013*)

The structure of a forest canopy is the key determinant of light transmission, use and understory availability. Airborne light detection and ranging (LiDAR) has been used successfully to measure multiple canopy structural properties, thereby greatly reducing the fieldwork required to map spatial variation in structure. However, lidar metrics to date do not reflect the full extent of the three-dimensional information available from the data. To this end, we developed a new metric, the polar grid fraction (GRID), based on gridding lidar returns in polar coordinates, in order to more closely match measurements provided by field instruments on leaf area index (LAI), gap fraction (GF) and percentage photosynthetically active radiation transmittance (tPAR). The metric summarizes the arrangement of lidar point returns for a single ground location rather than to an area surrounding the location.

Compared with more traditional proportion-based and height percentile-based estimators, the GRID estimator increased validation R^2 by 14.5% for GF and 6.0% for tPAR over the next best estimator. LAI was still best estimated with the more traditional statistic based on the proportion of ground returns in 14 m × 14 m moving kernels. By applying the models to a 2 × 2 m grid across the lidar coverage area, extreme values occurred in the estimations of all three response variables when using proportion-based and height percentile-based estimators. However, no extreme values were estimated by models using the GRID estimator, indicating that models based on GRID may be less influenced by spurious data. These results suggest that the GRID estimator is a strong candidate for any project requiring estimates of canopy metrics for large areas.

1. Introduction

Forest canopy structure imparts major functional controls over light use and transmission as well as gas fluxes and exchanges with the atmosphere. Hence, the high variation in canopy structure even across small spatial areas can drive variation in a wide range of ecological processes, such as forest productivity, seedling regeneration, plant morphology, nutrient cycling and plant succession patterns (Field 1988; Chen and Klinka 1997; Beaudet and Messier 1998; Montgomery and Chazdon 2001; Théry 2001). Accordingly, a great effort has been directed at quantifying spatial variation in canopy structure and the associated light regimes in forest ecosystems.

*Corresponding author. Email: nvaughn@carnegiescience.edu

Leaf area index (LAI), the total leaf surface area per unit area on the ground, and gap fraction (GF), the proportion of the sky view at a given point occluded by vegetation, are related by way of leaf orientation in spherical space and degree of clumping (Campbell and Norman 1989). Field instruments such as the LAI-2000 (LI-COR Biosciences Inc., Lincoln, Nebraska, NE, USA) can be used to indirectly estimate LAI by direct estimation of GF using some assumptions made about spatial arrangement and leaf angle distribution. While GF and LAI measure physical traits of the canopy, the fraction of absorbed photosynthetically active radiation (fPAR) directly measures the effect of the canopy on stand lighting conditions. fPAR is strongly related to productivity, indicating the efficiency at which a canopy uses the incoming radiation (Ter-Mikaelian et al. 1999). One can obtain direct estimates of fPAR by pairing two matching sensors, such as the AccuPAR LP-80 (Decagon Devices Inc., Pullman, Washington, WA, USA), with one placed outside the influence of the canopy. Summarizing multiple readings from these sensors, it is easy to get stand-level estimates of these structural variables, but understanding the spatial variation of such values requires an immense effort to gather the required amount of data (Asner, Sourlook, and Hioke 2003).

An alternative approach is to use estimates of canopy structure derived from airborne light detection and ranging (lidar). Popular lidar-derived metrics for estimating canopy structure are built from the proportion of returns falling under different classifications, such as ground, vegetation, first, last and single (Morsdorf et al. 2006; Solberg et al. 2009; Richardson and Moskal 2011), or from sample statistics of the lidar return height distribution (Riaño et al. 2004; Peduzzi et al. 2012). However, such metrics derive from the vertical distribution of points alone, and they do not take into account the horizontal distribution of return points. In essence, they can provide estimates of canopy cover, an area metric, rather than canopy closure – the mean of GF across all zenith angles – which is a point metric (Korhonen et al. 2011).

Field instruments such as the LAI-2000 are designed to measure point metrics of canopy structure by sampling across a wide range of zenith angles, rather than by sampling vertical angles alone. Because canopy structure can vary over short distances, these point estimates can also be highly variable over short distances on the ground (Bequet et al. 2012). This leads to the question of whether a lidar metric that incorporates the spatial information from individual returns within this hemispherical sample space can improve the precision of model estimates of canopy structure. To answer this question, we developed a new metric based on a binning of lidar returns into a grid defined by regular intervals of polar coordinates. This polar grid fraction (GRID) was designed to more closely match the angular sampling of these field instruments. Here, we present this new metric, and we report on improvements in estimation against two more traditional metrics, when all are tested across a naturally fragmented tropical montane forest landscape where canopy characteristics are highly spatially variable. Additionally, we apply this new model estimator over a wide range of input values to examine its stability for extrapolation purposes.

2. Methods

2.1. Study site

The study site is located on the northeast slope of the Mauna Loa volcano approximately 30 km west from the city of Hilo, Hawaii. The tropical montane forests of this area were fragmented by two lava flows in 1855 and 1881, resulting in a mosaic of open lava and remnant fragments of varying size (<0.1 to >200 ha) as well as some reshaped, but still

Table 1. Descriptive statistics of the three response variables from individual instrument samples measured along transects in the study area. Leaf area index (LAI), gap fraction (GF) and percentage transmitted photosynthetically active radiation (tPAR) are from the individual LAI-2000 and AccuPAR LP-80 readings taken in the field. Canopy height (CH) is from the CH model grid cells within which the geolocated field transect sample points fall. LAI and GF each have a sample size of 618, whereas tPAR has a sample size of 858.

Statistic	LAI	GF	tPAR (%)	CH (m)
Minimum	0.3	0.01	0.4	0.0
1st quartile	2.4	0.07	5.2	7.9
Median	3.3	0.13	9.7	12.2
Mean	3.5	0.17	13.4	12.5
3rd quartile	4.5	0.23	17.6	17.2
Maximum	7.9	0.86	89.0	31.0
Std. Deviation	1.5	0.14	12.3	6.0
Coefficient of variation	0.4	0.83	0.9	0.5

contiguous forest. Elevation for the studied fragments, which are dominated by the canopy tree *Metrosideros polymorpha* Gaud (ohia lehua), ranges from 1400 to 2000 m. Many of the fragments also include scattered individuals of the canopy tree *Acacia koa* A. Gray (koa), whereas the mid-story and understory of all fragments are made up of just a few species of trees and shrubs (Flaspohler et al. 2010). All species are evergreen deciduous. Over the many decades of isolation, edge effects have resulted in forest characteristics that vary widely across and within the different fragments. The combination of a simple and uniform flora, long-term nature of fragmentation, high degree of replication (>150 fragments examined), widely ranging fragment size, relative isolation from human influence and current protection in a State of Hawaii forest reserve has created a unique model ecological system for understanding the effects of fragmentation on forest structure and function. Descriptive statistics for LAI, GF, tPAR and canopy height (CH) from across the study area are listed in Table 1.

2.2. Field data collection

The field survey was performed during the months of June through October 2011. We established 29 transects that each bisected one of the forest fragments within the study area. Transect length ranged from 40 m to 362 m, depending on the forest fragment size and transect orientation. The transects were intentionally placed through regions of highly variable CH, using *a-priori* visual inspection of CH maps derived from lidar data. Transect endpoints were georeferenced using a GEO XT GPS unit (Trimble Navigation, Ltd., Sunnyvale, CA, USA) with post-processed accuracy of 1 m. Field crews recorded the position along the transect tapes, while taking single measurements from the LAI-2000 to estimate GF and LAI. Spacing between samples was determined *a priori* and took one of four values, 5, 10, 15 or 20 m, whichever most closely matched the lidar-derived local CH. So spacing under a 16 m canopy would be 15 m. Additionally, single measurements from the AccuPAR LP-80 instrument were done to estimate canopy percentage transmittance of photosynthetic light, defined as 1 minus fPAR. Sample spacing with this instrument was every 5 m along the same transects, regardless of CH. After collection and removal of obvious errors, 618 valid LAI-2000 samples, each containing both LAI and GF estimates, and 858 valid LP-80 samples containing tPAR remained.

2.3. Lidar data collection

On 10 and 13 January 2008, the Carnegie Airborne Observatory (CAO) Beta system (Asner et al. 2007) (http://cao.ciw.edu) was flown over the area at a height of 2500 m above ground level at an average speed of about 75 knots (38.6 m/s). The CAO-Beta lidar was a custom-built system with a laser beam divergence of 0.56 mrad and a laser wavelength of 1064 nm. For this data collection, the lidar pulse frequency was set to 33 kHz, and scan frequency to 10 Hz. While the CAO typically has full-waveform functionality, for this mission, only up to four discrete return pulses were utilized. These flight and instrument settings yielded a data set of 1.17 returns/m^2, on average, over the vegetated area.

2.4. Polar grid fraction metric

We developed a new method to estimate the three canopy structural variables. Our new method closely matches the three-dimensional sampling approach of the LAI-2000 instrument, which reads light intensity using a hemispherical light-sensor in five concentric bands of width 15°. Specifically, we took advantage of the simple mapping of a Cartesian coordinate direction vector – that from a single return to a given three-dimensional sample location – into azimuth (θ) and zenith (φ) polar angles. The angles for all returns surrounding a given sample point can then be binned into a two-dimensional grid defined by intervals of θ (wedges) and φ (rings), rather than the traditionally used x (columns) and y (rows). A visualization of such a grid is pictured in Figure 1. A given cell in this polar grid can be marked as 'hit' if the (θ,φ) angle pairs representing one or more lidar returns fall within the angle intervals defining the cell. After evaluating all returns, the fraction of hit cells should relate strongly to canopy closure. However, the two values will differ by stand type, as different species have different leaf and branch properties that will affect how light is scattered. Terrestrial laser scanners also record in polar coordinates, and such data have been used to estimate GF and LAI (Danson et al. 2007; Vaccari et al. 2013).

The LAI-2000 reads GF values using five bands of approximately 15° each. In a similar manner, we grouped multiple rings into bands of about 15° each. We used the first four such bands, covering the range 0–60°. The range of the azimuth angle, θ, was divided into 16 equal wedges of 22.5° each. Unlike in traditional grids, polar grid cell size increases with φ and with distance from origin. Larger cells have a larger probability of containing returns. While we can't account for distance, the effect of φ can be nullified by defining ring intervals in the scale of cos φ. In this study, they were intentionally placed through regions of highly variable CH, and the range of this transformed zenith angle was broken into rings of width 0.0175. Thus, in φ scale, the zenith angle interval for ring r is given by $\arccos(1 - 0.0175(r - 1)) \leq \varphi < \arccos(1 - 0.0175r)$. Regular steps in cos φ scale do not line up directly with the desired 15° wide bands, so the nearest available ring boundary was used. As a result, band intervals were marginally narrower or wider than 15°.

Due to air turbulence during flight and multiple overlaps of flight lines, the density of the lidar data set was variable in some regions. This was found to affect the GRID estimator, as more points increase the chance that a polar grid cell will be occupied. To correct for this, the lidar data set was systematically thinned such that there were no more than four returns in any 2 × 2 m grid cell. If more than four returns existed, only four returns, randomly selected from those available, were retained. Using the thinned lidar data set, we then produced a 2 × 2 m raster data set, (RGRID), covering the entire study area and containing one layer for each of the four bands of GRID values. GRID values were computed at the centre point of each 2 × 2 m cell.

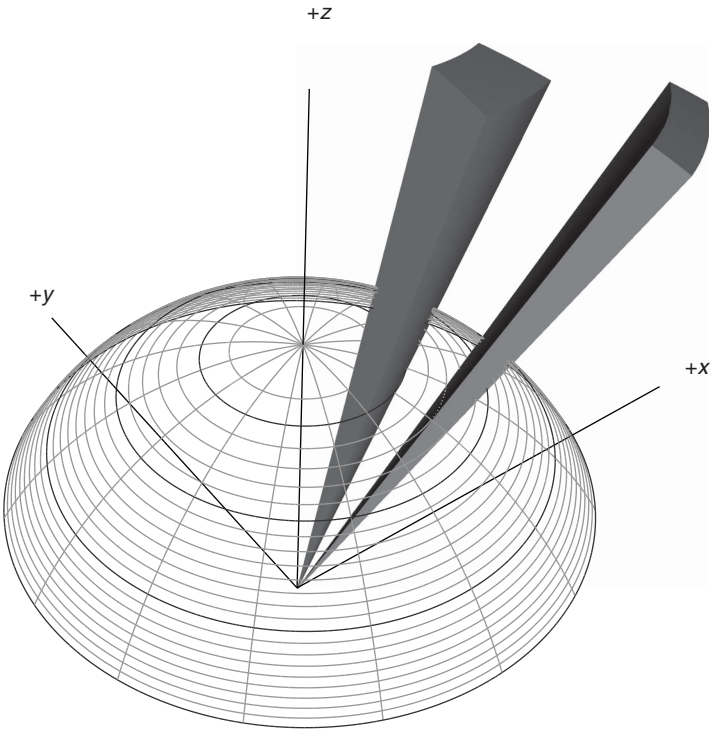

Figure 1. A graphical representation of the polar grid used to estimate gap fraction from the lidar data. As in this study, there are 16 azimuth angle wedges and 24 zenith angle rings. Cells are a combination of ring and wedge, akin to row and column of *x*-*y* grids. Boundaries of the four 15° wide bands are depicted with darker lines. All cells within each band were used to compute the polar grid fraction for this band. Truncated volumes of space depicting the projection from the origin of two individual grid cells are depicted. The end surface area of such volumes is equal at a given radius from the origin (instrument sample point) for all cells because rings are defined by intervals in cos φ scale.

2.5. Other lidar-based metrics

We desired to compare our polar grid statistics against the more traditional techniques. In most cases, this involves collecting all lidar returns falling within a given window surrounding each sample location. Statistics are computed for a subset of these points and used as independent variables in modelling the crown structure metric of interest. Metrics may incorporate the return order along pulse information (e.g. first, last, only) or the ground-vs.-canopy classification of each return. Morsdorf et al. (2006) provided one such metric – the number of first returns divided by the number of first and second returns – that should be linearly related to LAI assuming a spherical foliage distribution. Solberg et al. (2009) provided two more examples designed to estimate LAI by way of its link to GF. The first, given in Equation (1), is the ratio of the count of returns classified as ground, n_g, to the total count of all ground and canopy, n_c, returns. This is essentially a measure of the mean areal GF if considering only near-vertical zenith angles. A second version incorporates the within-pulse order of each return as well. The extra information was unnecessary in our case, and T was the best performer of all three proportion-based metrics considered. Though originally designed for a model in which both GF and T are log-transformed, better results were achieved without these transformations on our data set.

$$T = n_g/(n_g + n_c). \quad (1)$$

We computed T for each 2 × 2 m cell in a regular grid covering the study area, using all returns collected within a 14 × 14 m window centred on each 2 × 2 m grid cell. The proportion T is the proportion (PROP) estimator. As with the GRID values, this single value was stored in a second raster data set (RPROP).

Other metrics can be based on the return height distribution, such as height percentiles. These have been shown to be effective in determining structure and structural class of stand development (Riaño et al. 2004; Jones et al. 2012; Peduzzi et al. 2012). For all returns falling within the same 14 × 14 m window, a script collected and sorted these values to compute percentile statistics for the distribution of return heights. We created a third estimator set, PERC, by computing the 25th, 50th, 75th, 90th and 95th percentiles using all the return heights within each window. A third raster data set (RPERC) with 2 × 2 m cell resolution was created to store these values.

2.6. Crown structure modelling

We tested the capabilities of the three lidar-derived metrics – GRID, PROP and PERC – as estimators when applied to model each of the three canopy metrics – LAI, GF and tPAR – as responses. For each field sample point, we matched the measured value to the RGRID, RPROP and RPERC values for the 2 × 2 m cell within which the sample point is contained. Thus, we created nine new vectors of estimated responses, one for each of the estimator–response combinations.

To ensure that we tested estimation performance rather than simply model fit performance, we tested the efficacy of each estimator group using a k-fold cross-validation procedure. In this procedure, the data set is divided into k groups. The estimated values for each group are then obtained by applying a model fit to the samples from all $(k - 1)$ remaining groups. In this way, no models are trained with and applied to the same datum. We used five groups, such that about 20% of the data was randomly placed into each group. The LAI-2000 samples were divided into four groups of 124 samples each, and one group of 122. The LP-80 samples were, likewise, divided into three groups of 172 samples, and two groups of 171 samples.

For each such vector, the coefficient of determination, R^2, was computed using Equation (2). The validation root mean square error (RMSE) was also computed using Equation (3). Both equations incorporate the combined estimations from all $k = 5$ groups. Here, n is the number of samples in group i, p is the number of terms in the model for a given estimator set, y_{ij} is the measured response variable and x_{ij} is the vector of measured estimator variables of record j in group i, $\bar{y}$ is the mean of the response variable over all records, and $f_{\sim i}$ is the least squares regression function fit to all records not in group i.

$$R^2 = 1 - \frac{\sum_{i=1}^{k}\sum_{j=1}^{n_i}[y_{ij} - f_{\sim i}(\mathrm{x}_{ij})]^2}{\sum_{i=1}^{k}\sum_{j=1}^{n_i}[y_{ij} - \bar{y}]^2}, \quad (2)$$

$$\mathrm{RMSE} = \sqrt{\frac{\sum_{i=1}^{k}\sum_{j=1}^{n_i}[y_{ij} - f_{\sim i}(\mathrm{x}_{ij})]^2}{\sum_{i=1}^{k}[n_i] - p}}. \quad (3)$$

2.7. Model sensitivity

Overly sensitive models may produce invalid estimates given input values slightly outside the range in the training data. We were interested in the behaviour of the estimators in regions with low representation in the training data. We applied the five different models created during the cross-validation procedure for each of the nine combinations of estimator and response variable to all grid cells in the appropriate raster data set. After combining the results across all five cross-validation models, we computed the range and the first and third quartiles for each of the nine estimator–response combinations. In doing so, any extreme values estimated could be compared between estimators, and the sensitivity of the given models at each extreme could be assessed.

3. Results

The validation R^2 increased and the RMSE values decreased significantly when using the GRID estimator set for response variables GF and tPAR (Table 2). The proportion-based estimator, PROP, performed best for LAI as a response variable. R^2 ranged from 0.211 to 0.245 for GF, 0.229 to 0.281 for LAI and 0.241 to 0.354 for tPAR. The improvement in R^2 over the next best estimator, PERC, was 14.5% for estimating GF and 6.0% for estimating tPAR. These coincide with reductions of 2.1% and 1.6% in RMSE, respectively. GRID outperformed PROP in R^2 for GF and tPAR by 16.1% and 47.9%, respectively. On the other hand, the PROP estimator outperformed GRID for estimating LAI by 14.7%. For estimating tPAR, the PROP estimator did poorly by comparison, with the largest R^2 reaching 0.241.

Interquartile ranges of the values obtained by applying the three estimator sets to the entire raster data sets (Table 3) were not far from those observed with the field instruments (Table 1). Extremely large or small values, such as LAI of –6.4 or tPAR of –10.9 were most common for the PERC estimator (Table 3). Use of the PROP estimator resulted in estimates as low as −2.8 for LAI. The GRID estimator set was the most stable, producing no extreme values for any of the response variables.

4. Discussion

The use of the GRID estimator set yielded improved precision over the PROP and PERC sets when estimating the GF and tPAR canopy structure variables. This is especially true

Table 2. Statistics from the $k = 5$ cross-validation runs on each response variable combined with each estimator variable set. R^2 is from Equation (2) and RMSE is from Equation (3).

Response	Estimator set	R^2	RMSE
GF	GRID†	0.245	0.1224
GF	PERC†	0.214	0.1251
GF	PROP†	0.211	0.1249
LAI	GRID	0.245	1.324
LAI	PERC	0.229	1.339
LAI	PROP	0.281	1.289
tPAR	GRID	0.354	9.935
tPAR	PERC	0.334	10.094
tPAR	PROP	0.241	10.747

Note: †Number of variables per estimator set: GRID, 4, PERC, 5 and PROP, 1.

Table 3. The range, and first and third quartiles of estimations when applying each model during the cross-validation procedure to all valid cells across the study area in the appropriate raster data sets. This shows the stability of the estimators when applied to more extreme data than that found in the training set.

Response	Raster	Minimum	1st quartile	3rd quartile	Maximum
GF	RGRID	0.050	0.107	0.249	0.340
GF	RPERC	−0.046	0.110	0.237	0.938
GF	RPROP	0.017	0.131	0.247	0.665
LAI	RGRID	1.73	2.61	4.17	4.87
LAI	RPERC	−6.44	2.72	4.16	6.31
LAI	RPROP	−2.79	2.53	3.97	5.42
tPAR	RGRID	3.4	7.5	21.7	34.1
tPAR	RPERC	−10.9	7.4	20.5	40.3
tPAR	RPROP	−0.6	10.2	21.1	61.0

for the tPAR variable over the PROP set. The key difference of the GRID metric is that the GRID values are specific to a given sample point, whereas proportions and distribution percentile values apply to a fixed area. This difference suggests that the GRID estimator set can explain more of the between-sample point variation in structure metric readings, potentially producing a more accurate fine-scale map of canopy structure.

While using the GRID set did improve estimates over the PERC set, the PROP set performed best for estimating LAI. Due to the negative log-transformation of GF required to compute LAI from GF analysis, small changes in GF near zero result in large changes in LAI values. The poor results in GF may indicate that values of the GRID may have been too saturated near zero to differentiate these higher LAI values, and this would be most prominent in the outside bands. The largest GRID-estimated LAI value is 4.87 (Table 3), significantly lower than those for the other two estimators. If this is discovered to be an underestimate, one possible correction may be to further reduce the polar grid cell dimensions (by reducing θ and φ angle steps). This would increase the number of cells to improve the resolution for lower grid fraction values.

The R^2 values presented here are low compared with values presented in other publications using estimators similar to PROP or PERC. For example, Morsdorf et al. (2006) modelled LAI using proportions with an adjusted R^2 of 0.69, whereas Solberg et al. (2009) modelled LAI (via GF) using proportion ratios with an R^2 of up to 0.92. Using the 75th height percentile, Riaño et al. (2004) found a correlation coefficient of up to 0.95 with LAI. There are several possible reasons for these lower R^2 values. First, and probably most important, we are modelling single field instrument readings rather than averaged values from several readings taken at each plot. The *M. polymorpha* canopy is non-uniform, and instrument readings are highly variable within a small area. These single readings are also more difficult to accurately locate with a GPS equipment. Second, previously reported values of R^2 result from model fitting analysis and not from model validation analysis. Estimations from a model nearly always have larger residuals when applied to new data, and some of the R^2 difference seen here represents this effect of regression modelling.

Two other factors, site characteristics and lidar return density, may affect estimator performance in models. For example, model performance in efforts to estimate canopy structure metrics can vary widely across forest types (Riaño et al. 2004; Jensen et al. 2008; Hopkinson and Chasmer 2009). In one case, model performance declined with increasing

LAI (Jensen et al. 2008). The high elevation, tropical forest examined produces a large range in LAI values. Also, the density of returns in our lidar data set is lower than normal for missions flown in the year 2008. Thomas et al. (2006) found that a reduction in lidar return density hampered stand-level crown closure estimations. Similar results should be expected for other canopy structure metrics.

An important property of any estimator when applied to large landscapes is that it should not produce extreme values when extrapolated. In this regard, the GRID estimator excelled, producing no extremes for any response metric. In contrast, the PROP and especially the PERC estimators behaved poorly on the outer limits of the ranges of all three canopy structure metrics, indicating that these approaches may not be appropriate for all data conditions.

The polar grid metric shows promise as a precise and accurate estimator of canopy structure metrics. We showed that improvement in estimation precision was significant for the GF and tPAR canopy metrics, and that the metric was insensitive to slight extrapolation. It is possible that improvements could be even greater, and perhaps even hold for LAI, when applied to lidar data of higher density and GPS positioning of higher accuracy. Ultimately, these improvements could lead to improved modelling of large-scale forest canopy structure and processes such as productivity. Further, modelling for an individual point rather than for an area, fine-scale spatial analysis of canopy and stand characteristics is possible.

Acknowledgements

We thank Ty Kennedy-Bowdoin, other Carnegie Airborne Observatory staff members, and Devin Leopold for assistance with airborne lidar data collection, processing and analysis. We thank Bernice Hwang, Tony Kovach, Colin Phifer, and Britney Sung for field measurements. We thank the University of Hawai‘i at Hilo for access to GPS equipment, and the State of Hawaii Division of Forestry and Wildlife for access to field sites. Funding for this research was provided by National Science Foundation grant DEB-0715593 (GPA), the Carnegie Institute of Science and the USDA Forest Service Pacific Southwest Research Station as part of a larger project funded by National Science Foundation grants DEB-1020412 (T. Fukami, CPG, GPA), DEB-1020007 (D.S. Gruner), and DEB-1019928 (D.J. Flaspohler). The Carnegie Airborne Observatory is made possible by the Gordon and Betty Moore Foundation, the John D. and Catherine T. MacArthur Foundation, Avatar Alliance Foundation, W.M. Keck Foundation, the Margaret A. Cargill Foundation, Grantham Foundation for the Protection of the Environment, Mary Anne Nyburg Baker, G. Leonard Baker Jr., and William R. Hearst III.

References

Asner, G. P., D. E. Knapp, T. Kennedy-Bowdoin, M. O. Jones, R. E. Martin, J. Boardman, and C. B. Field. 2007. “Carnegie Airborne Observatory: In-Flight Fusion of Hyperspectral Imaging and Waveform Light Detection and Ranging for Three-Dimensional Studies of Ecosystems.” *Journal of Applied Remote Sensing* 1: 013536.

Asner, G. P., J. M. O. Sourlook, and J. A. Hioke. 2003. “Global Synthesis of Leaf Area Index Observations: Implications for Ecological and Remote Sensing Studies.” *Global Ecology and Biogeography* 12: 191–205.

Beaudet, M., and C. Messier. 1998. “Growth and Morphological Responses of Yellow Birch, Sugar Maple, and Beech Seedlings Growing Under a Natural Light Gradient.” *Canadian 340 Journal of Forest Research* 28: 1007–1015.

Bequet, R., M. Campioli, V. Kint, B. Muys, J. Bogaert, and R. Ceulemans. 2012. “Spatial Variability of Leaf Area Index in Homogeneous Forests Relates to Local Variation in Tree Characteristics.” *Forest Science* 58: 633–640.

Campbell, R. G., and J. M. Norman. 1989. “The Description and Measurement of Plant Canopy 345 Structure.” In *Plant Canopies: Their Growth, Form, and Function*, edited by G. Russel, B. Marshall, and P. G. Jarvis, 1–19. Cambridge: Cambridge University Press.

Chen, H. Y. H., and K. Klinka. 1997. "Light Availability and Photosynthesis of Pseudot-Suga Menziesii Seedlings Grown in the Open and in the Forest Understory." *Tree Physiology* 17: 23–29.

Danson, F. M., D. Hetherington, F. Morsdorf, K. Benjamin, and B. Allgower. 2007. "Forest Canopy Gap Fraction From Terrestrial Laser Scanning." *IEEE Transactions on Geoscience and Remote Sensing* 4: 157–160.

Field, C. B. 1988. "On the Role of Photosynthetic Responses in Constraining the Habitat Distribution of Rainforest Plants." *Functional Plant Biology* 15: 343–358.

Flaspohler, D. J., C. P. Giardina, G. P. Asner, P. Hart, J. Price, C. K. Lyons, and X. Castaneda. 2010. "Long-Term Effects of Fragmentation and Fragment Properties on Bird Species Richness in Hawaiian Forests." *Biological Conservation* 143: 280–288.

Hopkinson, C., and L. Chasmer. 2009. "Testing LiDAR Models of Fractional Cover Across Multiple Forest Ecozones." *Remote Sensing of Environment* 113: 275–288.

Jensen, J. L. R., K. S. Humes, L. A. Vierling, and A. T. Hudak. 2008. "Discrete Return Lidar-Based Prediction of Leaf Area Index in Two Conifer Forests." *Remote Sensing of Environment* 112: 3947–3957.

Jones, T. G., N. C. Coops, and T. Sharma. 2012. "Assessing the Utility of LiDAR to Differentiate Among Vegetation Structural Classes." *Remote Sensing Letters* 3: 231–238.

Korhonen, L., I. Korpela, J. Heiskanen, and M. Maltamo. 2011. "Airborne Discretereturn LIDAR Data in the Estimation of Vertical Canopy Cover, Angular Canopy Closure and Leaf Area Index." *Remote Sensing of Environment* 115: 1065–1080.

Montgomery, R. A., and R. L. Chazdon. 2001. "Forest Structure, Canopy Architecture, and Light Transmittance in Tropical Wet Forests." *Ecology* 82: 2707–2718.

Morsdorf, F., B. Kotz, E. Meier, K. I. Itten, and B. Andallgower. 2006. "Estimation of LAI and Fractional Cover From Small Footprint Airborne Laser Scanning Data Based on Gap Fraction." *Remote Sensing of Environment* 104: 50–61.

Peduzzi, A., R. H. Wynne, T. R. Fox, R. F. Nelson, and V. A. Thomas. 2012. "Estimating Leaf Area Index in Intensively Managed Pine Plantations Using Airborne Laser Scanner 375 Data." *Forest Ecology and Management* 270: 54–65.

Riaño, D., F. Valladares, S. Condes, and E. Chuvieco. 2004. "Estimation of Leaf Area Index and Covered Ground from Airborne Laser Scanner (Lidar) in Two Contrasting Forests." *Agricultural and Forest Meteorology* 124: 269–275.

Richardson, J. J., and L. M. Moskal. 2011. "Strengths and Limitations of Assessing Forest Den-
380 Sity and Spatial Configuration with Aerial LiDAR." *Remote Sensing of Environment* 115: 2640–2651.

Solberg, S., A. Brunner, K. H. Hanssen, H. Lange, E. Næsset, M. Rautiainen, and P. Stenberg. 2009. "Mapping LAI in a Norway Spruce Forest Using Airborne Laser Scanning." *Remote Sensing of Environment* 113: 2317–2327.

Ter-Mikaelian, M. T., R. G. Wagner, F. W. Bell, and C. Shropshire. 1999. "Comparison of Photosynthetically Active Radiation and Cover Estimation for Measuring the Effects of Interspecific Competition on Jack Pine Seedlings." *Canadian Journal of Forest Research* 29: 883–889.

Théry, M. 2001. "Forest Light and Its Influence on Habitat Selection." *Plant Ecology* 153: 251–261.

Thomas, V. A., P. Treitz, J. H. Mccaughey, and I. Morrison. 2006. "Mapping Stand-Level Forest Biophysical Variables for a Mixedwood Boreal Forest Using Lidar: An Examination of Scanning Density." *Canadian Journal of Forest Research* 36: 34–47.

Vaccari, S., M. V. Leeuwen, K. Calders, N. C. Coops, and H. Martin. 2013. "Bias in Lidar- 395 Based Canopy Gap Fraction Estimates." *Remote Sensing Letters* 4: 391–399.